NASA Technical Memorandum 101313
AIAA-88-2815

Investigation of Oscillating Cascade Aerodynamics by an Experimental Influence Coefficient Technique

Lewis Research Center
Cleveland, Ohio

and

Sanford Fleeter
Purdue University
West Lafayette, Indiana

Presented at the
24th Joint Propulsion Conference
cosponsored by the AIAA, ASME, SAE, and ASEE
Boston, Massachusetts, July 11-13, 1988

NASA

INVESTIGATION OF OSCILLATING CASCADE AERODYNAMICS BY AN EXPERIMENTAL INFLUENCE COEFFICIENT TECHNIQUE

Daniel H. Buffum
National Aeronautics and Space Administration
Lewis Research Center
Cleveland, Ohio 44135

Sanford Fleeter
Thermal Sciences and Propulsion Center
School of Mechanical Engineering
Purdue University
West Lafayette, Indiana 47907

Abstract

Fundamental experiments are performed in the NASA Lewis Transonic Oscillating Cascade Facility to investigate the torsion mode unsteady aerodynamics of a biconvex airfoil cascade at realistic values of the reduced frequency for all interblade phase angles at a specified mean flow condition. In particular, an unsteady aerodynamic influence coefficient technique is developed and utilized in which only one airfoil in the cascade is oscillated at a time and the resulting airfoil surface unsteady pressure distribution measured on one dynamically instrumented airfoil. The unsteady aerodynamics of an equivalent cascade with all airfoils oscillating at a specified interblade phase angle are then determined through a vector summation of these data. These influence coefficient determined oscillating cascade data are correlated with data obtained in this cascade with all airfoils oscillating at several interblade phase angle values. The influence coefficients are then utilized to determine the unsteady aerodynamics of the cascade for all interblade phase angles, with these unique data subsequently correlated with predictions from a linearized unsteady cascade model.

Nomenclature

C	airfoil chord
C_m	unsteady moment coefficient about midchord
C_m^n	unsteady aerodynamic moment influence coefficient for n^{th} airfoil
C_p	unsteady pressure coefficient, $p_1/\frac{1}{2}\rho V^2\alpha_1$
C_p^n	unsteady pressure influence coefficient for n^{th} airfoil
k	reduced frequency, $\omega C / 2 V$
M	inlet Mach number
p_1	first harmonic of airfoil surface unsteady static pressure
S	airfoil spacing
V	inlet velocity
x	chordwise coordinate
y	coordinate normal to chordwise direction
α_o	mean flow incidence angle
α_1	torsional oscillation amplitude
γ	stagger angle
ΔC_p	unsteady pressure difference coefficient
β	interblade phase angle (positive when airfoil i leads airfoil n-1)
ρ	inlet density
τ	maximuim airfoil thickness
ω	airfoil oscillatory frequency

Introduction

In the rotating blade rows of turbomachines and propellers, the possibility of flutter is a continual concern. Unfortunately, the ability to predict flutter has not kept pace with the overall advances and new requirements of turbomachine and turboprop designs. Consequently, the development of analyses to predict oscillating cascade aerodynamics is of fundamental research interest. To direct the development of these advanced unsteady aerodynamic models and to evaluate these as well as existing analyses, data from oscillating cascade experiments are needed. However, due to the complexity of these experiments, few results are available at realistic reduced frequency values, particularly in the high subsonic and transonic flow regimes.

Oscillating cascade experiments are complex and time consuming because the unsteady aerodynamics of the cascade must be measured, not only for every new steady flow condition and reduced frequency, but also for each interblade phase angle value. In principle, however, oscillating cascade data can be obtained for all interblade phase angles at a specified mean flow condition and reduced frequency through simpler experiments. In particular, an unsteady aerodynamic influence coefficient technique can be utilized when the unsteady disturbances are small, such as in the flutter stability problem. In this technique, only one airfoil in the cascade is oscillated, with the resulting airfoil surface unsteady pressure distributions measured on the oscillating airfoil and its stationary neighbors. The unsteady aerodynamics of an equivalent cascade with all airfoils oscillating at a specified interblade phase angle are then determined through a vector summation of these influence coefficient data.

To utilize this unsteady aerodynamic influence technique to acquire unsteady aerodynamic data which the designer and analyst will use, it is first necessary to experimentally verify the validity of this technique. This requires the correlation of oscillating cascade data determined from the unsteady aerodynamic influence coefficients with corresponding data for a cascade in which all airfoils oscillate at specific interblade phase angles. Several investigations have been directed at this

experimental verification. However, the results are inconclusive. Hanamura, Tanaka and Yamaguchi [1] had good results using the influence coefficient technique, but their experiment, performed in a water channel, was limited to incompressible flow. Davies and Whitehead [2] performed such experiments in an annular cascade at high subsonic inlet conditions and reduced frequencies up to 0.1. Unfortunately, the validity of the unsteady aerodynamic influence technique cannot be assessed due to the data scatter. The effect of oscillating a single airfoil and three airfoils in a cascade at low speed was studied by Tanaka, Yamamoto, and Fujimoto [3]. Although a summation of the influence coefficients was not presented, the technique appears promising for data in regions of attached flow. In supersonic inlet Mach number experiments at ONERA [4], the summation of influence coefficients has been compared to data for a linear cascade with two airfoils oscillating. The limited scope of these experiments precludes conclusions concerning the validity of the influence coefficient technique.

In this paper, the NASA Lewis Transonic Oscillating Cascade Facility is utilized to investigate the torsion mode unsteady aerodynamics of a biconvex airfoil cascade at realistic values of the reduced frequency for all interblade phase angles at a specified mean flow condition. This is accomplished by: (1) experimentally verifying the unsteady aerodynamic influence coefficient technique; (2) subsequently utilizing this experimental technique to determine the unsteady aerodynamics of an oscillating cascade for all interblade phase angles. In particular, in a subsonic compressible flow at realistic reduced frequencies, unsteady aerodynamic influence coefficient data are obtained by oscillating one airfoil in the cascade and measuring the resulting airfoil surface unsteady pressure distributions on the oscillating airfoil and its stationary neighbors. These unique data are correlated with the corresponding oscillating cascade data, i.e., data obtained in this cascade with all airfoils oscillating at several interblade phase angle values. The unsteady aerodynamic influence coefficients are then utilized to determine the unsteady aerodynamics of the cascade for all interblade phase angles, with these unique data subsequently correlated with predictions from a linearized unsteady cascade model.

Theory

Figure 1 schematically depicts the two-dimensional finite cascade representation of a rotor blade row. For a given mean flow field and reduced frequency of oscillation, the cascade unsteady aerodynamics can be written in terms of linearly combined influence coefficients which can be determined both experimentally and analytically.

For a finite airfoil cascade with 2N+1 airfoils executing constant amplitude harmonic oscillations with a constant interblade phase angle, β, the unsteady aerodynamic moment, C_m, acting on the reference airfoil, taken as airfoil 0 for convenience, can be expressed as a Fourier series of the influence coefficients, $\bar{C}_m^n$, Equation 1. These influence coefficients can be experimentally measured in a finite cascade by oscillating a single airfoil and measuring the unsteady aerodynamics on the oscillating airfoil and its stationary neighbors.

$$C_m(\beta) = \sum_{n=-N}^{N} \bar{C}_m^n \, e^{in\beta} \qquad (1)$$

where $\bar{C}_m^n$ are the complex unsteady aerodynamic moment influence coefficients which define the unsteady moment developed on the reference airfoil due to the motion of airfoil n with all of the other airfoils in the cascade stationary.

Mathematical models for an infinite cascade of airfoils oscillating with a specified interblade phase angle can also be used to determine these unsteady aerodynamic influence coefficients. For this case, the number of airfoils is taken as infinite, with the influence coefficients subsequently determined by the inversion of Equation 1.

$$\bar{C}_m^n = \frac{1}{2\pi} \int_{-\pi}^{\pi} C_m(\beta) e^{-in\beta} \, d\beta \qquad (2)$$

Analytically determined unsteady aerodynamic influence coefficients can thus be determined from oscillating cascade mathematical models by integrating over the complete interblade phase angle interval, Equation 2. Utilizing these influence coefficients in Equation 1 then enables analytical results for a finite number of airfoils oscillating in an infinite cascade to be determined.

Oscillating Cascade Facility

The NASA Lewis Transonic Oscillating Cascade Facility shown in Figure 2 is a linear cascade wind tunnel capable of test section Mach numbers approaching unity. Air drawn from the atmosphere passes through a smoothly contracting inlet section, into a constant area 9.78 cm by 19.21 cm test section and then through a diffuser and exhaust header which has a nominal pressure of 3.0 N/cm^2. The flow rate is controlled by two valves located in the header. Upstream of the test section, a partitioned bleed system removes the boundary layers on each end wall. The boundary layers on the upper and lower cascade walls are removed through tailboard slots.

A major feature of this facility is the high speed mechanical drive system which imparts controlled torsional oscillations to any or all of the nine cascaded airfoils. Nine barrel cams, each with a six cycle sinusoidal groove machined into its periphery, are mounted on a common shaft driven by a 74.6 kW electric motor. Connecting arms, joined to one end of each airfoil by trunnions, have buttons on the opposite end to follow the cam grooves. The amplitude of the airfoil motion is ± 1.2 degrees, dictated by the cam and follower geometry. With all of the airfoils oscillating, different interblade phase angle oscillations are achieved by changing the relative positions of the cams. In this investigation, the maximum oscillatory frequency is 350 Hz, corresponding to a reduced frequency of 0.390 with a cascade inlet Mach number of 0.65.

Airfoils and Instrumentation

The cascade is comprised of nine uncambered biconvex airfoils with a chord of 7.62 cm, a thickness-to-chord ratio of 0.076, a solidity of 1.3, and a 53 degree stagger angle. The radius of curvature of the airfoil surfaces is 27.4 cm, with the leading and trailing edges rounded with a 0.025 cm radius of curvature. The

airfoils are supported by two midchord trunnions, resulting in a midchord elastic axis location.

The primary data are the complex unsteady surface pressures on the oscillating cascaded airfoils. These data are obtained by six Kulite transducers flush mounted symmetrically along the chord on one airfoil surface, Table 1, and then statically calibrated. Thus, to obtain the unsteady pressure data for both surfaces during simultaneous oscillation of the airfoils, the experiments are performed in two phases with data acquired on one surface at a time. The transducers, each with an active sensor diameter of 0.097 cm, 1.3% of the airfoil chord, are placed in milled slots and potted in RTV to isolate them from airfoil strain. For the influence coefficient experiments, a thin coating of RTV protects the sensor surface and fairs it into the contour of the airfoil.

During oscillation, the pressure transducers are subject to accelerations which may produce significant apparent pressure signals. To quantify this effect, the instrumented airfoil was oscillated at several frequencies under no-flow or zero mean velocity conditions. Figure 3 shows the amplitude response of the six coated transducers as a function of the acceleration magnitude. The response is a linear function of the acceleration, implying that the acoustic response, which is expected to vary with the airfoil velocity magnitude, is dominated by the acceleration response. Significant amplitude variation is apparent among the transducers, and is probably due to installation effects. The phase angle variation with frequency was linear and small for all the transducers.

The time-variant position of the reference oscillating airfoil is determined by a capacitance-type proximity sensor which produces a voltage proportional to the air gap between it and an adjacent object. This sensor is positioned to face a six cycle sinusoidally-shaped cam mounted on the same shaft as the airfoil drive cams and to be in phase with the reference airfoil motion. As shown in the sample in Figure 4, this signal is virtually noise-free.

Data Acquisition and Analysis

All of the unsteady signals are a.c. coupled and recorded on magnetic tape for post-experiment processing. During tape playback, the signals are simultaneously digitized at rates sufficient to capture at least three harmonics of the oscillation frequency, with 32,768 samples taken per channel. Each data channel is divided into blocks, typically with 2048 samples, and then Fourier decomposed and referenced to the airfoil motion by subtracting the phase of the motion signal from the pressure signal. With all of the transducer signal blocks decomposed, the results are averaged and, in the case of the influence coefficient data, the acceleration responses are subtracted vectorally. To minimize errors due to spectral leakage, an interpolation scheme is applied to the decomposed results in conjunction with a Hanning window [5].

To demonstrate this data analysis technique, the pressure transducer signals shown in Figure 4 are considered. The resulting averaged pressure spectra, Figure 5, are characterized by a large spike at the oscillation frequency, in this case 200 Hz, some small spikes at higher harmonics of the oscillation frequency, and other small spikes caused by wind tunnel tones.

The final unsteady pressure data are defined by the complex dynamic pressure and pressure difference coefficients, C_p and ΔC_p, Equation 3. These complex data are presented in the format of a magnitude and phase referenced to the airfoil motion, with a positive phase corresponding to the unsteady pressure leading the airfoil motion.

$$C_p(x) = \frac{p_1(x)}{\frac{1}{2}\rho V^2 \alpha_1} \; ; \; \Delta C_p = C_{pl} - C_{pu} \tag{3}$$

where p_1 is the first harmonic of the unsteady static pressure, ρ and V are the inlet values of density and velocity, and α_1 is the torsional oscillation amplitude.

The summation of dynamic pressure coefficient influences is analogous to the moment coefficient summation of Equation 1. With $\bar{C}_p^n$ being the complex pressure influence coefficient, the dynamic pressure coefficient is calculated using Equation 4.

$$C_p(\beta) = \sum_{n=-N}^{N} \bar{C}_p^n e^{in\beta} \tag{4}$$

Torsion mode unsteady moment coefficients, C_m, are calculated from the unsteady pressure difference data, Equation 5. This is accomplished by: (1) assuming there is a zero pressure difference at the leading and trailing edges of the airfoil; (2) fitting a smooth curve through the chordwise distribution of the data; and (3) numerically integrating the resulting chordwise distribution of the pressure difference.

$$C_m = \int_0^1 \left(\frac{1}{2} - \frac{x}{C}\right) \Delta C_p d\left(\frac{x}{C}\right). \tag{5}$$

Results

The unsteady aerodynamic influence coefficient technique is experimentally investigated at steady flow conditions defined by an incidence angle of 0 degrees and an inlet Mach number of 0.65, resulting in an entirely subsonic flowfield. With the instrumented (reference) airfoil in Position 0 as defined in Figure 1, unsteady data are acquired on this airfoil with the airfoils in positions -2, -1, 0, +1, and +2 individually oscillating at reduced frequencies of 0.223 and 0.390. First the unsteady pressure influence coefficients on the individual surfaces of the reference instrumented airfoil are considered. These data are then correlated with: (1) predictions from the unsteady, small perturbation, subsonic flat plate cascade analyses of references 6 and 7; (2) baseline data obtained in experiments where all of the airfoils in the cascade are oscillating at the same time for interblade phase angles of 0, 90, and -90 degrees. In these experiments, the airfoil motion is defined by the change in the incidence angle with time:

$$\alpha(t) = \alpha_1 \mathrm{Re}\{e^{(i\omega t)}\} \tag{6}$$

α_1 is the oscillatory amplitude of 1.2 degrees and ω is the frequency.

Unsteady Airfoil Surface Influence Coefficients

Figures 6 through 10 present the chordwise distribution of the dynamic pressure influence coefficients on the individual surfaces of the Position 0 reference airfoil, with the oscillating airfoil in the five relative positions defined by -2 through +2.

The self-induced oscillating airfoil unsteady pressure response is shown in Figure 6. Namely, this figure presents the unsteady pressures on the surfaces of the reference airfoil, with the reference airfoil itself oscillating. The magnitude of the unsteady pressure on each surface attains a maximum at the leading edge, tending towards zero at the trailing edge, with the magnitude generally larger on the upper surface. Also, the upper surface phase data are out-of-phase with the airfoil motion.

Figures 7 and 8 show the unsteady pressure effect on the surfaces of the stationary instrumented reference airfoil due to individually oscillating its nearest neighbors, i.e., individually oscillating the airfoils in positions +1 and -1, respectively. As seen, oscillating the neighboring airfoil has a relatively large effect on the magnitude of the unsteady pressure on the reference airfoil surface nearest to the oscillating airfoil. In particular, Figure 7 shows that oscillating the airfoil located immediately above the reference airfoil results in relatively large unsteady pressure fluctuations over the aft half of the reference airfoil upper surface, with the lower surface pressure coefficient magnitude nearly constant and a nearly linear variation in the lower surface phase angle. With the oscillating airfoil positioned immediately beneath the reference airfoil, Figure 8 shows that there are relatively large pressure fluctuations over the leading quarter of the reference airfoil lower surface, while the upper surface has only a small response in the leading and trailing edge regions, with the lower surface oscillations out-of-phase with the motion.

The effect on the unsteady pressure on the surfaces of the instrumented reference airfoil due to oscillating the airfoils which are in the +2 and -2 positions are shown in Figures 9 and 10, respectively. As expected for this case with the oscillating airfoils further distanced from the reference airfoil, the magnitude of the unsteady pressures on the reference airfoil are reduced compared to the previous results where the nearest neighbors were oscillated. Also, with the oscillating airfoil above the reference airfoil in Position +2, the amplitudes are nearly the same for the two surfaces, but there is an unsteady load on the airfoil due to the phase difference at the two forward transducers, Figure 9. For the oscillating airfoil in Position -2, Figure 10 shows that the lower surface response is negligible while the upper surface has a small response over the forward two-thirds of the airfoil.

Unsteady Pressure Differences

The summation of the oscillating airfoil surface unsteady pressure influence coefficients and the determination of the unsteady pressure difference coefficient is shown in Figure 11. In particular, the 0.223 reduced frequency data are presented as a dynamic pressure difference coefficient for an interblade phase angle of 0 degrees, with N specifying the limits of the sum per Equation 4. Thus N = 0 corresponds to the self-induced unsteady aerodynamic response. The influence coefficient series is seen to be rapidly convergent, with only the reference airfoil and its two immediate neighbors having a significant effect on the resulting dynamic pressure difference distribution.

The influence coefficient determined chordwise distribution of the unsteady airfoil surface pressure difference data are correlated with corresponding data obtained in experiments in which all of the airfoils in the cascade are oscillating at the same time with a constant interblade phase angle value and also with the flat plate cascade predictions in Figures 12 through 14 at a 0.223 reduced frequency value and in Figures 15 through 17 for a reduced frequency of 0.390.

The complex unsteady aerodynamic influence coefficient data generally exhibit good correlation with both the oscillating cascade data and the linearized theory. In particular, the influence coefficient magnitude data either exhibit good correlation with both the oscillating cascade data and the prediction or else are centered between the two. The exceptions to this are the higher reduced frequency -90 and +90 degree interblade phase angle data, Figures 15 and 17. In these two cases, the influence coefficient magnitude data are either in good agreement or increased in value as compared to the oscillating cascade data, with both increased relative to the prediction.

The two sets of unsteady pressure difference phase data are in good agreement with one another and with the prediction at an interblade phase angle of -90 degrees, Figures 12 and 15. For in-phase motions, Figures 13 and 16 show that the two sets of phase data are decreased relative to the prediction, particularly at the higher reduced frequency, with the influence coefficient data centered between the prediction and the oscillating cascade data at 40% and 60% of chord. At an interblade phase angle of +90 degrees, Figures 14 and 17, the influence coefficient phase data are in good agreement with the prediction, with the oscillating cascade data increased in value.

Unsteady Aerodynamic Moment

Figures 18 and 19 show the measured and predicted complex unsteady aerodynamic moment influence coefficients for reduced frequencies of 0.223 and 0.390, respectively, in the format of the influence of the N^{th} airfoil in the cascade on the 0^{th} (reference) airfoil. The unsteady aerodynamic moment on the reference airfoil is seen to be a strong function of the unsteady aerodynamics associated with oscillating the reference airfoil itself and the two adjacent airfoils. Also, there is relatively good agreement between the measured and predicted influence coefficients for both reduced frequency values, as expected, for this zero incidence case with no shocks. However, there is better agreement between the prediction and the lower reduced frequency data. In particular, a comparison of these figures reveals that there is relatively poorer correlation between the prediction and the real component of the higher reduced frequency data for the influence of airfoils -1 and +2,

with the measured result larger in magnitude than predicted.

The resulting measured and predicted imaginary part of the unsteady aerodynamic moment on the reference airfoil of an infinite cascade for all interblade phase angles for reduced frequencies of 0.223 and 0.390 are presented in Figures 20 and 21, respectively. It should be noted that the influence coefficient data are valid for all interblade phase angles, forming a continuing curve with interblade phase angle value. Also shown are the -90, 0, and +90 degree interblade phase angle oscillating cascade data.

In general, there is good correlation between the influence coefficient data and the predictions for all interblade phase angles, with the lower reduced frequency data exhibiting somewhat better correlation as expected based on the previously presented influence coefficient data. The 90 degree interblade phase angle oscillating cascade data are greatly increased in value as compared to both the influence coefficient data and the predictions. For in-phase cascade oscillations, the influence coefficient data exhibit equally good correlation with the oscillating cascade data and the prediction, being centered between the two. For an interblade phase angle of -90 degrees, the two data sets and the predictions are in good agreement at the lower reduced frequency, with only the oscillating cascade data and the prediction in good agreement at the higher reduced frequency.

Figures 20 and 21 also present the theoretical results for the case of a finite number of oscillating airfoils in the cascade. For the subresonant interblade phase angles, the finite and infinite oscillating airfoil cascade predictions are in good agreement with one another. However, in the vicinity of the acoustic resonance points, the predictions are not in good agreement. In particular, to capture the rapidly changing unsteady aerodynamic response in these regions, many more oscillating airfoils in the finite cascade are required. Thus, acoustic resonances will not occur in linear cascade experiments due to the limited number of airfoils in the cascade.

Summary and Conclusions

A series of fundamental experiments have been performed in the NASA Lewis Transonic Oscillating Cascade Facility to investigate the torsion mode oscillating aerodynamics of a biconvex airfoil cascade. In particular, all interblade phase angles were considered at two realistic high values of the reduced frequency at specific subsonic zero incidence mean flow conditions. This was accomplished by developing and utilizing an unsteady aerodynamic influence coefficient technique in which only one airfoil in the cascade is oscillated and the resulting airfoil surface unsteady pressures measured on the oscillating airfoil and its stationary neighbors. Vector summation of these data allows determination of the unsteady aerodynamics for arbitrary interblade phase angles of an equivalent cascade with all airfoils oscillating.

Analysis of these unique data and correlation with both the predictions from the unsteady, small perturbation, subsonic flat plate cascade analyses and the baseline data obtained in experiments where all of the airfoils in the cascade are oscillating at the same time for interblade phase angles of 0, 90, and -90 degrees revealed the following.

* The unsteady aerodynamic influence coefficient series is rapidly convergent, with only the reference airfoil and its two immediate neighbors having a significant effect on the resulting unsteady pressure difference and aerodynamic moment coefficients.

* The complex unsteady pressure difference influence coefficient data generally exhibit good correlation with both the oscillating cascade data and the linearized theory. In particular, the influence coefficient magnitude data typically either exhibit good correlation with both the oscillating cascade data and the prediction or else are centered between the two.

* The linearized theory underpredicts the magnitude of the unsteady pressure difference coefficient in the airfoil leading edge region.

* With regard to the imaginary part of the unsteady aerodynamic moment, there is generally good correlation between the influence coefficient data and the prediction for all interblade phase angles, with the lower reduced frequency data exhibiting somewhat better correlation.

* The finite and infinite cascade oscillating airfoil predictions are in good agreement for subresonant interblade phase angles. However, in the vicinity of the acoustic resonance points, the two predictions are not in good agreement, with many more oscillating airfoils in the finite cascade required. Thus, acoustic resonances will not occur in linear cascade experiments due to the limited number of airfoils.

In summary, this unsteady aerodynamic influence coefficient experimental technique enables valid subsonic oscillating cascade data to be obtained at realistic values of the reduced frequency for all interblade phase angles. In particular, in terms of the interblade phase angle, the unsteady aerodynamic moment data are a continuous curve.

References

1. Hanamura, Y., Tanaka, H. and Yamaguchi, K., "A Simplified Method to Measure Unsteady Forces Acting on the Vibrating Blades in Cascade," *Bulletin of the JSME*, Vol. 23, No. 180, June 1980.

2. Davies, M.R.D. and Whitehead, D.S., "Unsteady Aerodynamic Measurements in a Transonic Annular Cascade," *Unsteady Aerodynamics of Turbomachines and Propellers*, Cambridge University, Cambridge, England, 1984.

3. Tanaka, H., Yamamoto, K. and Fujimoto, I., "Unsteady Aerodynamic Response of Cascade Blades in Pitching Oscillation with Flow Separation," *Unsteady Aerodynamics of Turbomachines and Propellers*, Cambridge University, Cambridge, England, 1984.

4. Szechenyi, E., "Fan Blade Flutter -- Single Blade Instability or Blade to Blade Coupling?", *ASME Paper 85-GT-216*, March 1985.

5. Burgess, J.C., "On Digital Spectrum Analysis of Periodic Signals," *Journal of the Acoustical Society of America*, Vol. 58, No. 3, September 1985.

6. Smith, S.N., "Discrete Frequency Sound Generation in Axial Flow Turbomachines," *Cambridge University Report CUED/A-Turbo/TR29*, 1971.

7. Fleeter, S., "Fluctuating Lift and Moment Coefficients for Cascaded Airfoils in a Nonuniform Compressible Flow," *AIAA Journal of Aircraft*, Vol. 10, No. 2, February 1973.

TABLE I. - AIRFOIL AND CASCADE GEOMETRY

Airfoil	
Type	biconvex, no chamber
Surface radius of curvature, cm	27.4
Leading and trailing edge radii of curvature, cm	0.025
Maximum airfoil thickness, τ, cm	0.58
Chord, C, cm	7.62
Elastic axis	midchord
Dynamic pressure transducer locations, percent chord	12, 25, 40, 60, 75, 88
Cascade	
Number of airfoils	9
Solidity, C/S	1.3
Spacing, S, cm	5.86
Stagger angle, γ, deg	53
Amplitude of motion, deg	$\pm$1.2

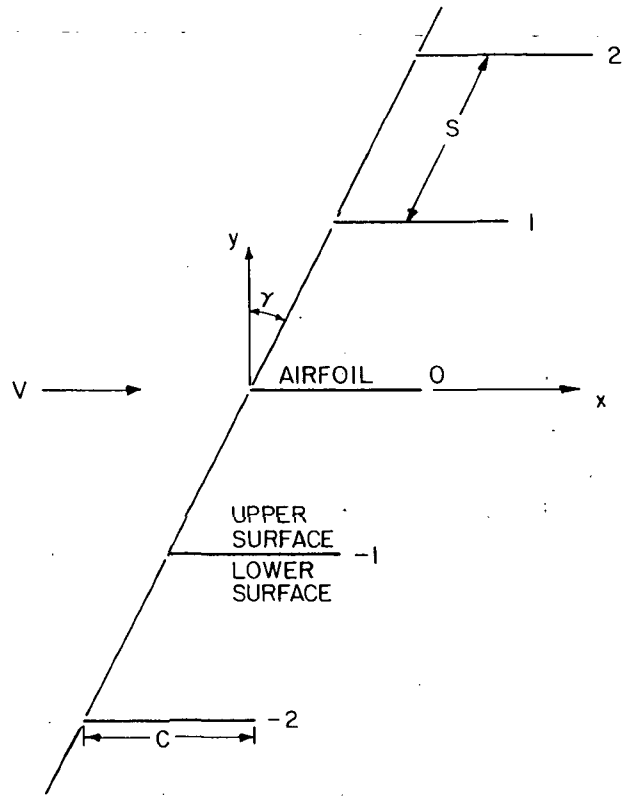

FIGURE 1. - CASCADE GEOMETRY.

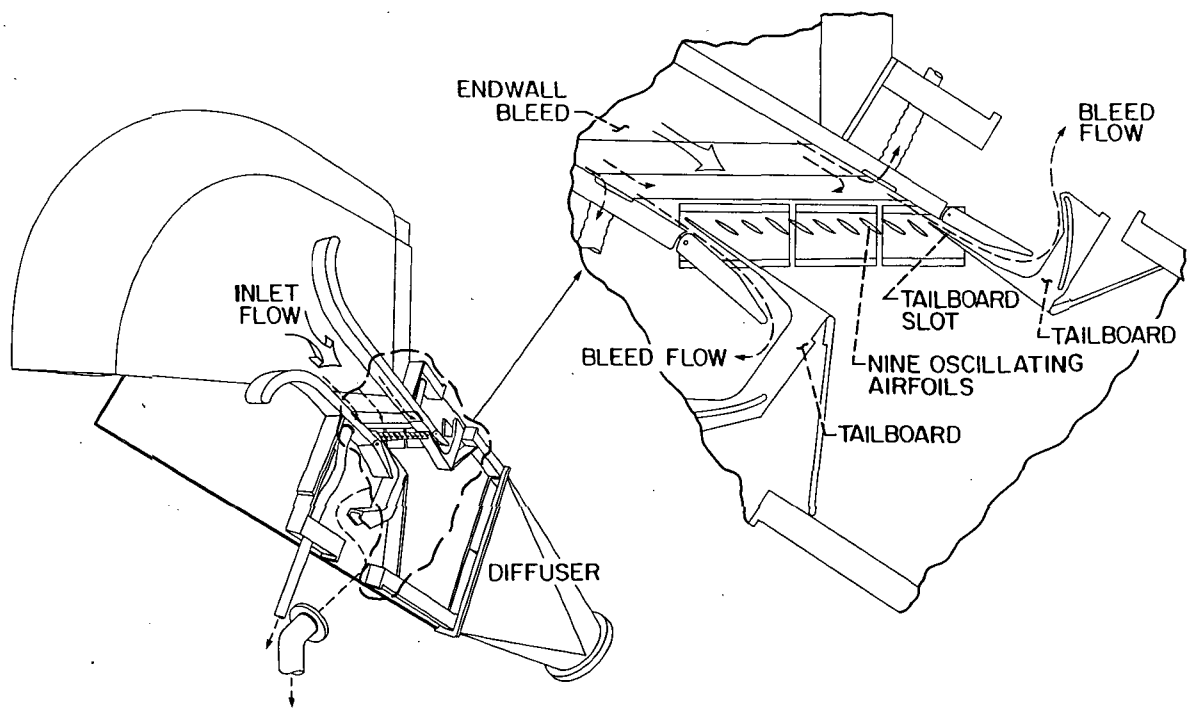

FIGURE 2. - NASA LEWIS TRANSONIC OSCILLATING CASCADE FACILITY.

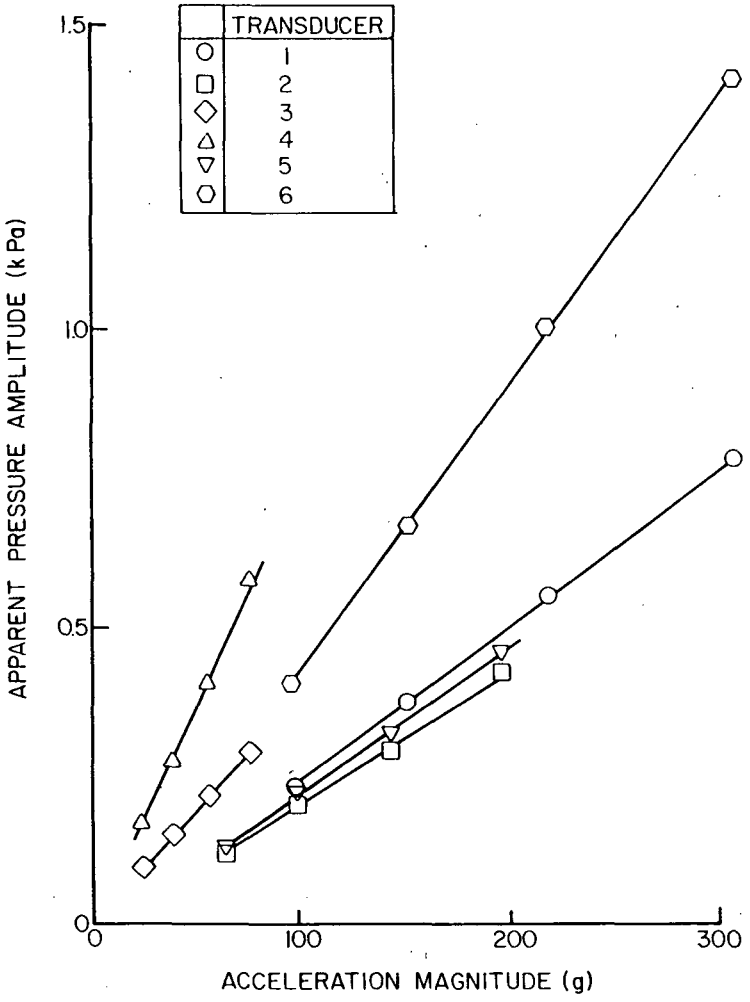

FIGURE 3. - DYNAMIC PRESSURE TRANSDUCER ACCELERATION RESPONSE.

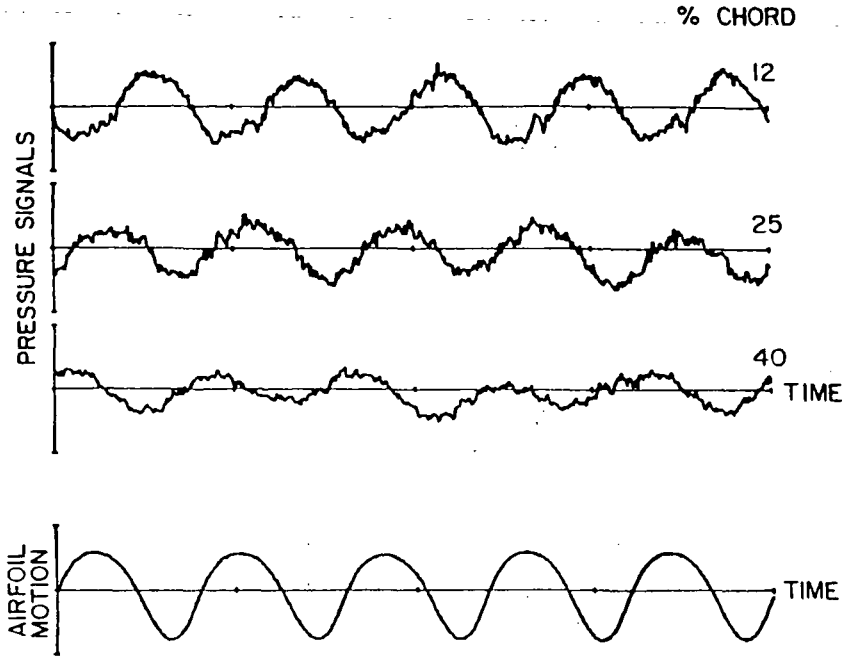

FIGURE 4. - TIME VARIANT SIGNALS.

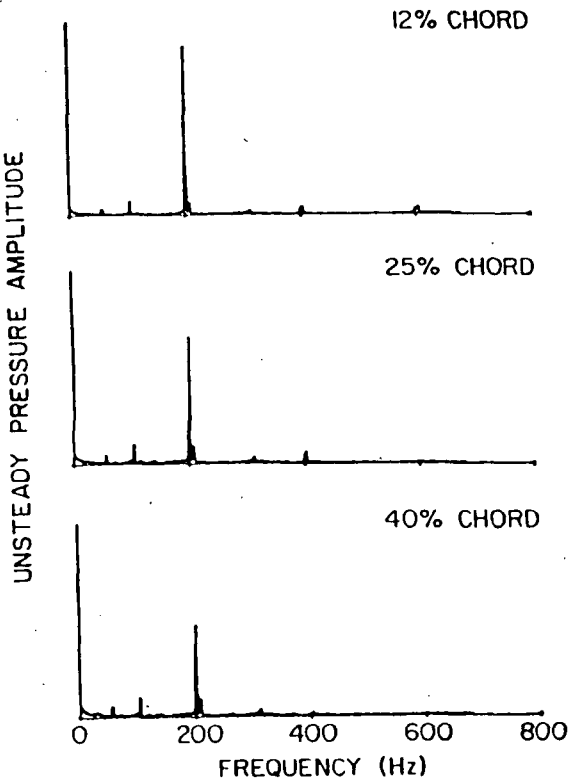

FIGURE 5. - AVERAGED PRESSURE SPECTRA.

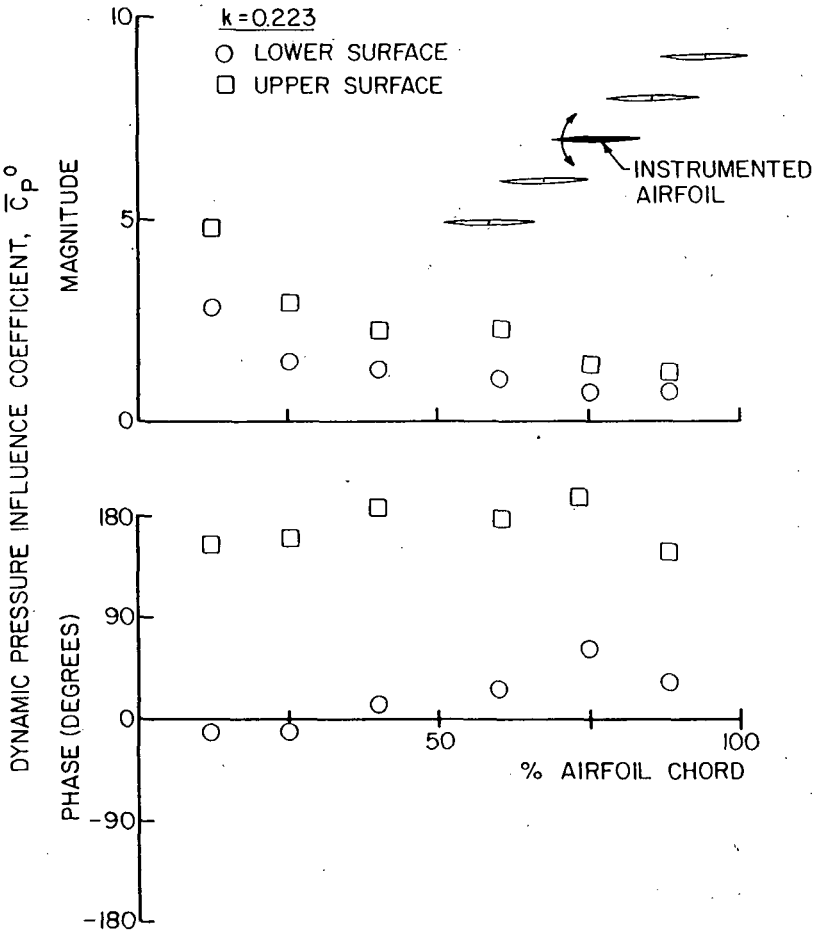

FIGURE 6. - DYNAMIC PRESSURE INFLUENCE COEFFICIENT, AIRFOIL 0 OSCILLATING.

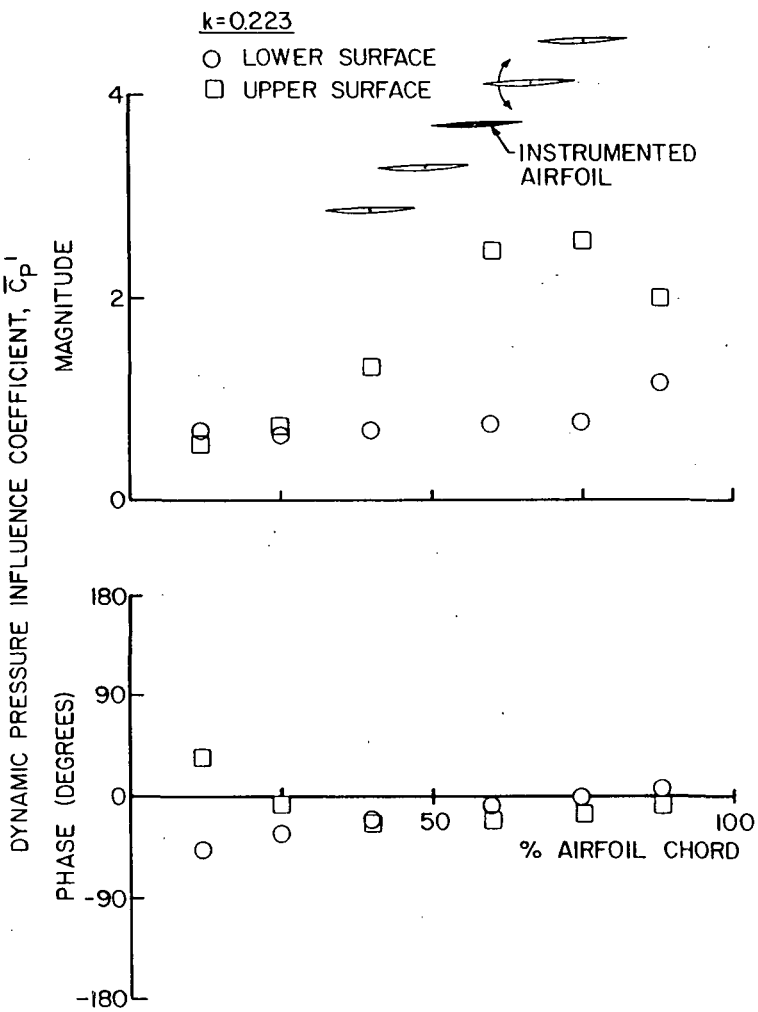

FIGURE 7. - DYNAMIC PRESSURE INFLUENCE COEFFICIENT, AIRFOIL 1 OSCILLATING.

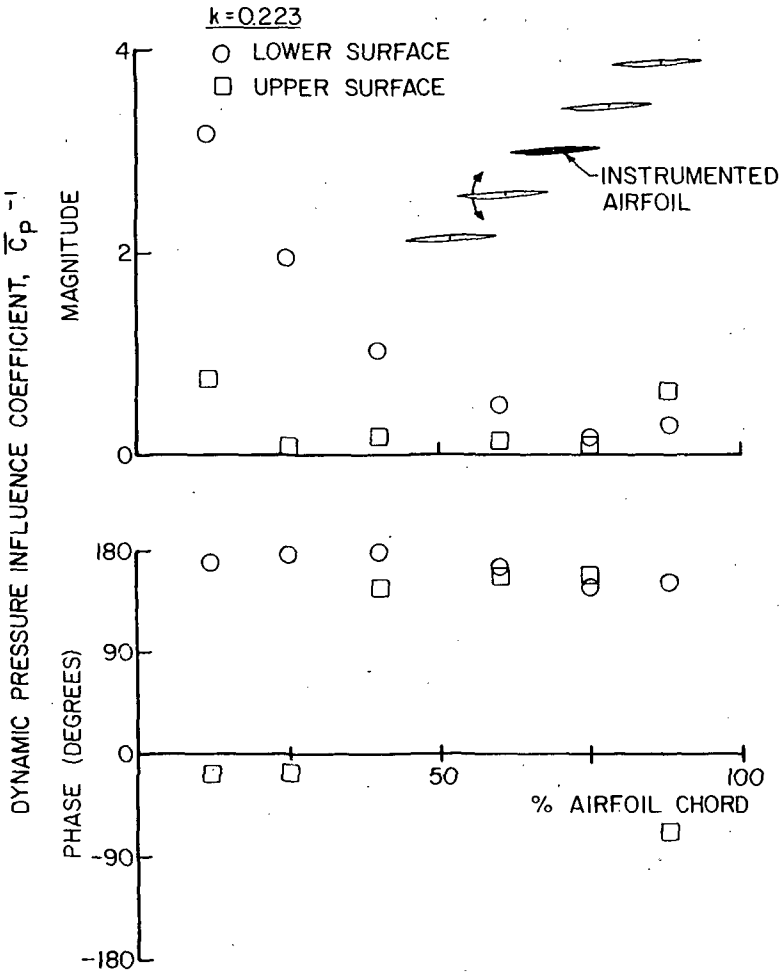

FIGURE 8. - DYNAMIC PRESSURE INFLUENCE COEFFICIENT, AIRFOIL -1 OSCILLATING.

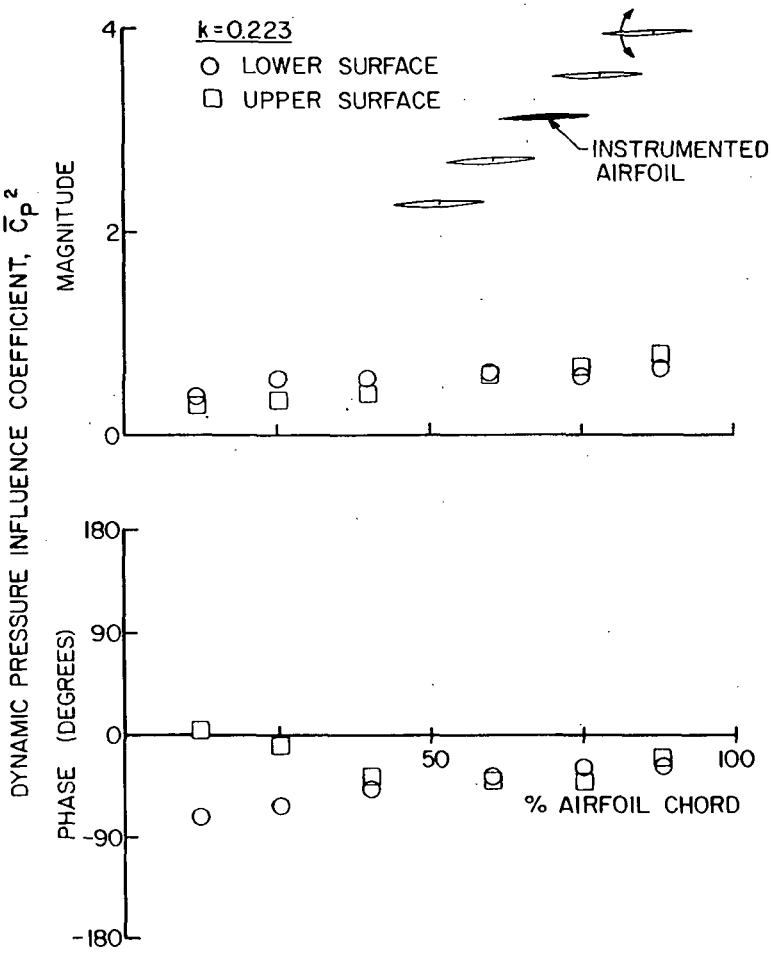

FIGURE 9. - DYNAMIC PRESSURE INFLUENCE COEFFICIENT, AIRFOIL 2 OSCILLATING.

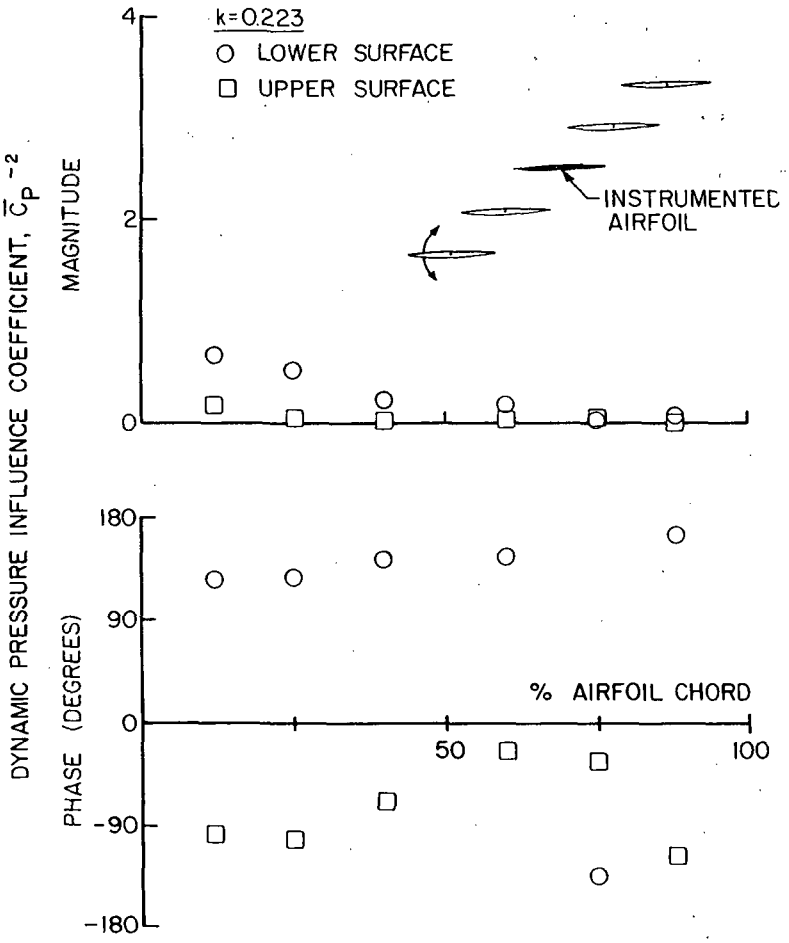

FIGURE 10. - DYNAMIC PRESSURE INFLUENCE COEFFICIENT, AIRFOIL -2 OSCILLATING.

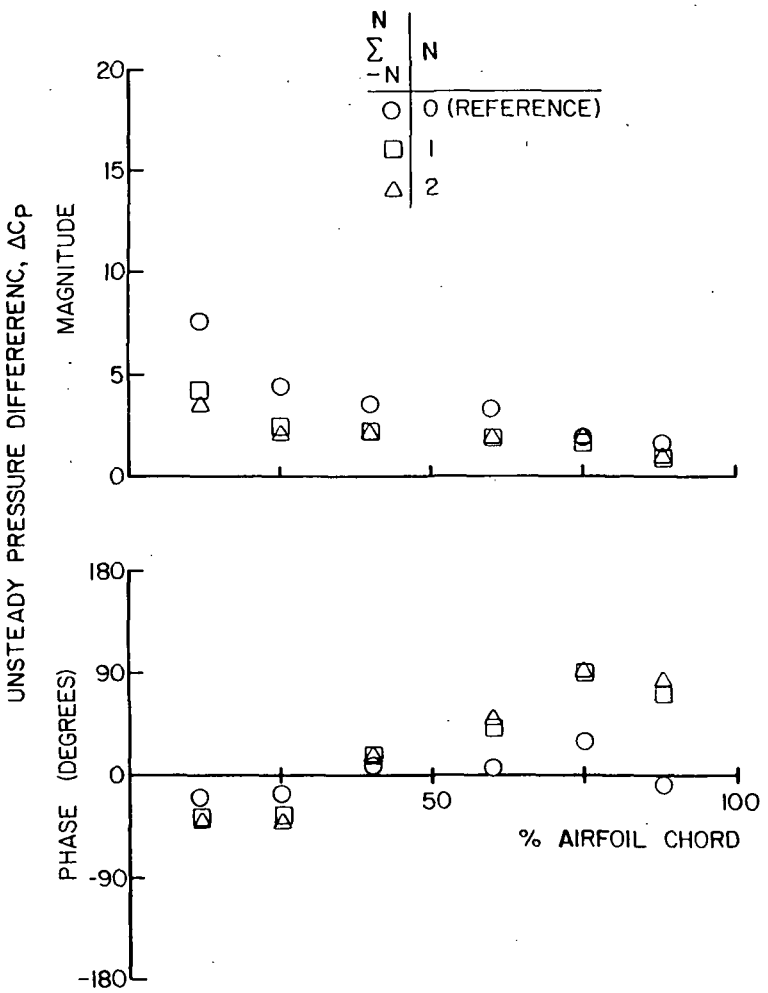

FIGURE 11. - UNSTEADY PRESSURE DIFFERENCE ON REFERENCE AIRFOIL, $\beta = 0^{0}$, $k = 0.223$.

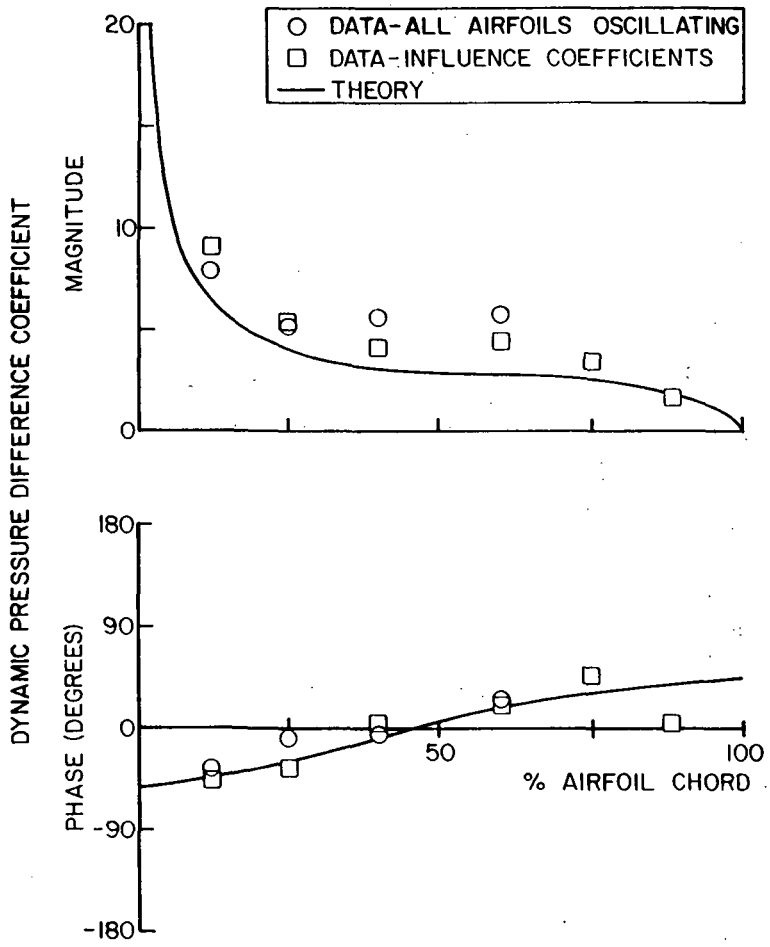

FIGURE 12. - DYNAMIC PRESSURE DIFFERENCE COEFFICIENT DISTRIBUTION, $\beta = -90^{0}$, $k = 0.223$.

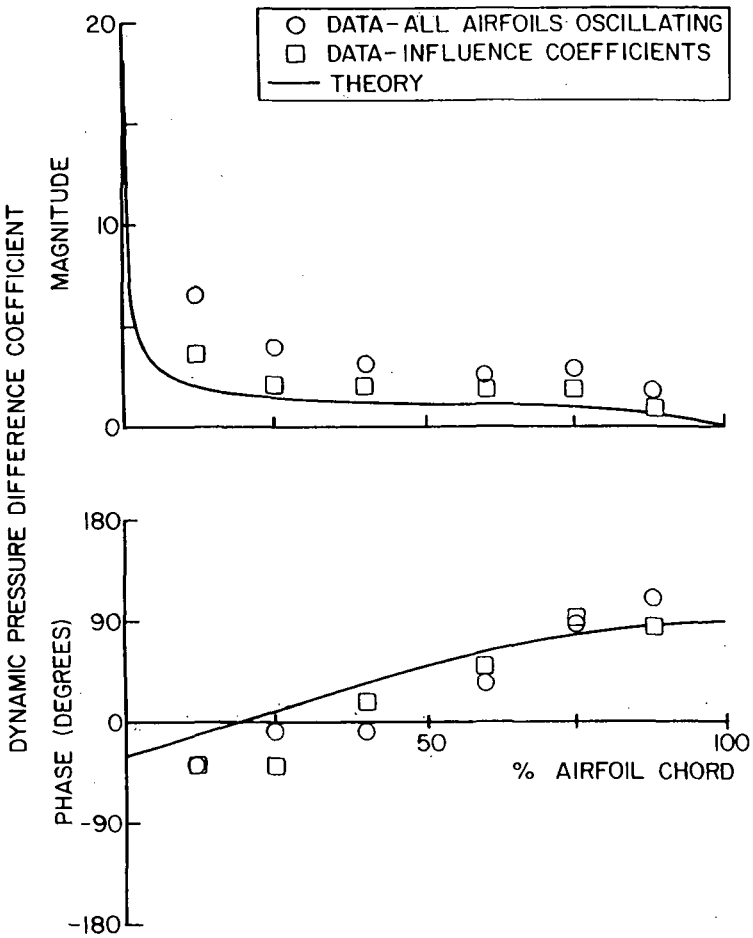

FIGURE 13. - DYNAMIC PRESSURE DIFFERENCE COEFFICIENT DISTRIBUTION, $\beta = 0^{0}$, $k = 0.223$.

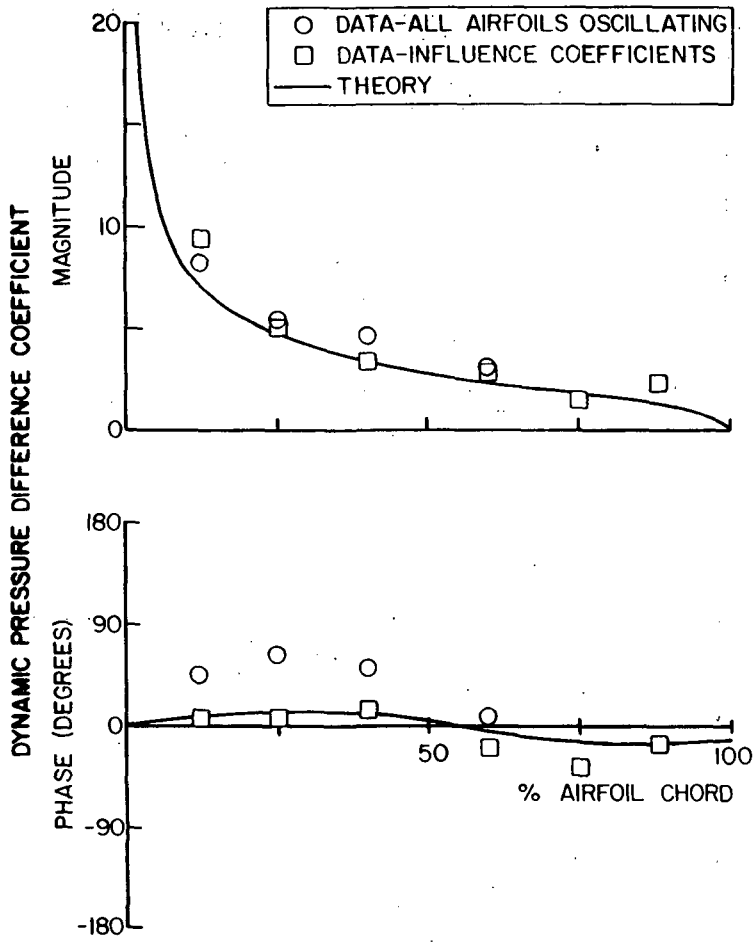

FIGURE 14. - DYNAMIC PRESSURE DIFFERENCE COEFFICIENT DISTRIBUTION, $\beta = 90^0$, $k = 0.223$.

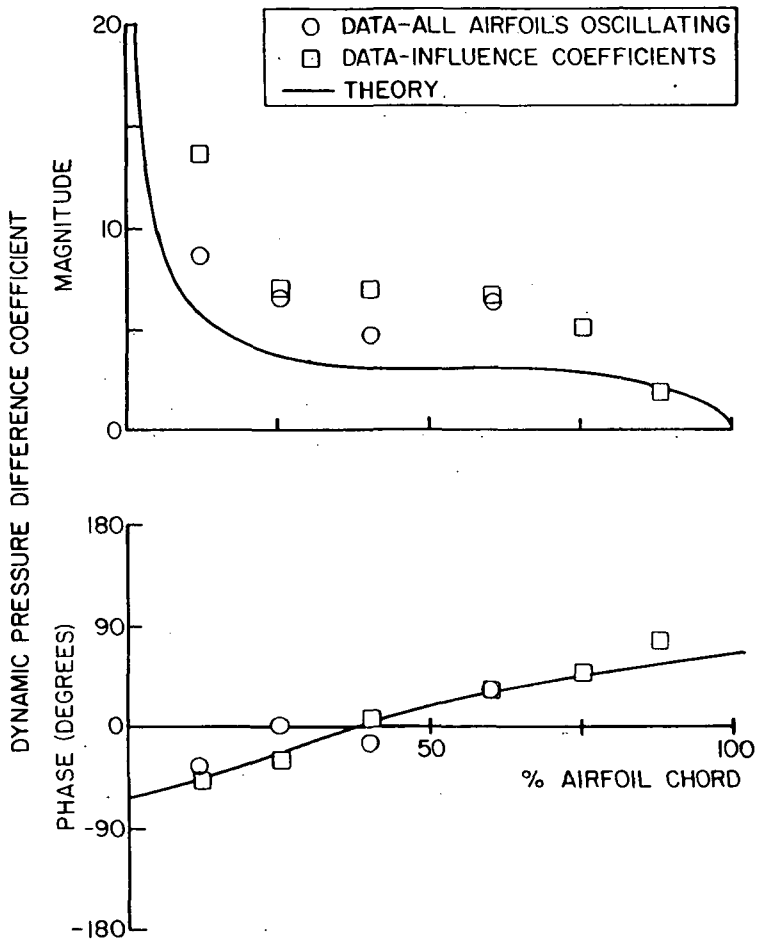

FIGURE 15. - DYNAMIC PRESSURE DIFFERENCE COEFFICIENT DISTRIBUTION, $\beta = -90^{0}$, $k = 0.390$.

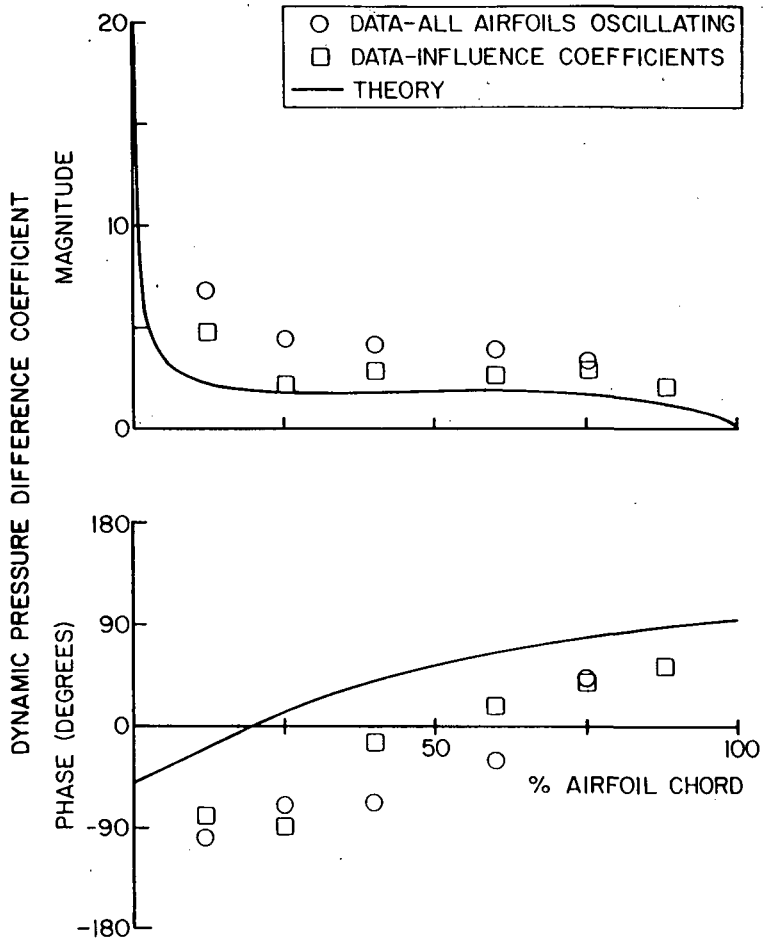

FIGURE 16. - DYNAMIC PRESSURE DIFFERENCE COEFFICIENT DISTRIBUTION, $\beta = 0^{o}$, $k = 0.390$.

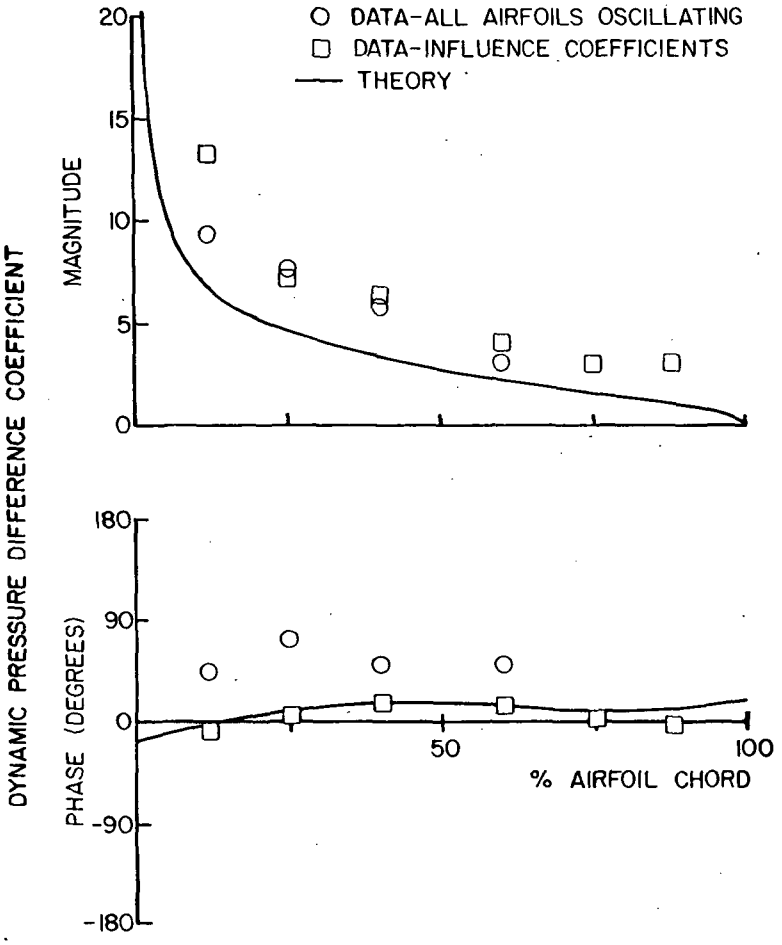

FIGURE 17. - DYNAMIC PRESSURE DIFFERENCE COEFFICIENT DISTRIBUTION. $\beta = 90^{0}$, $k = 0.390$.

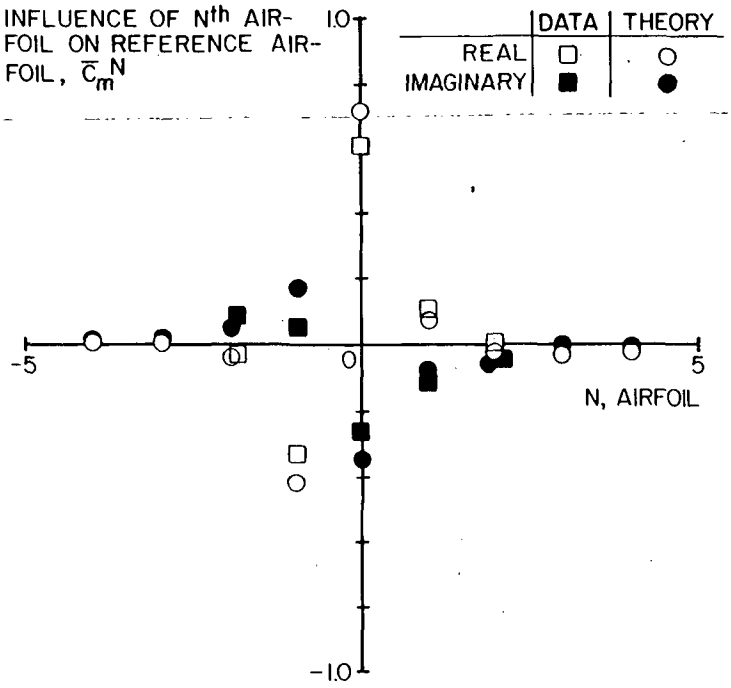

FIGURE 18. - INFLUENCE OF N^{TH} AIRFOIL ON REFERENCE AIRFOIL UNSTEADY AERODYNAMIC MOMENT, k = 0.223.

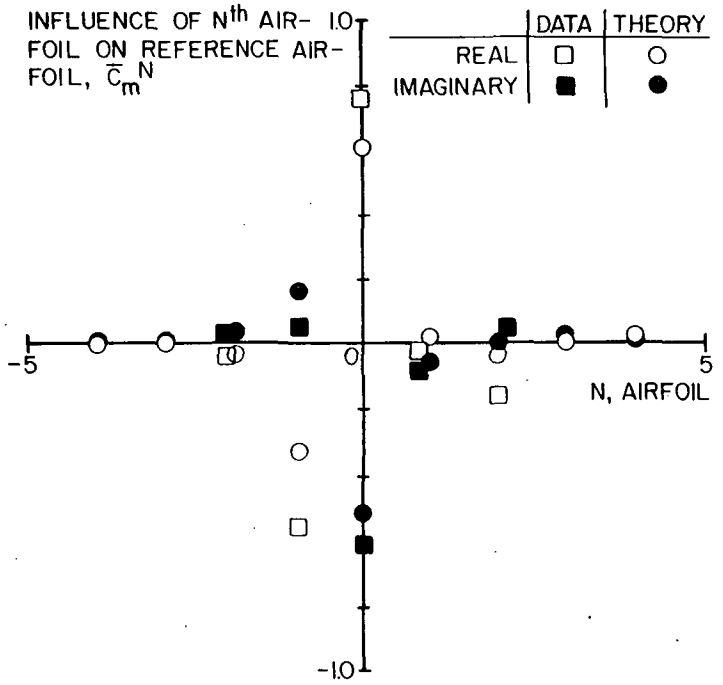

FIGURE 19. - INFLUENCE OF N^{TH} AIRFOIL ON REFERENCE AIRFOIL UNSTEADY AERODYNAMIC MOMENT, k = 0.390.

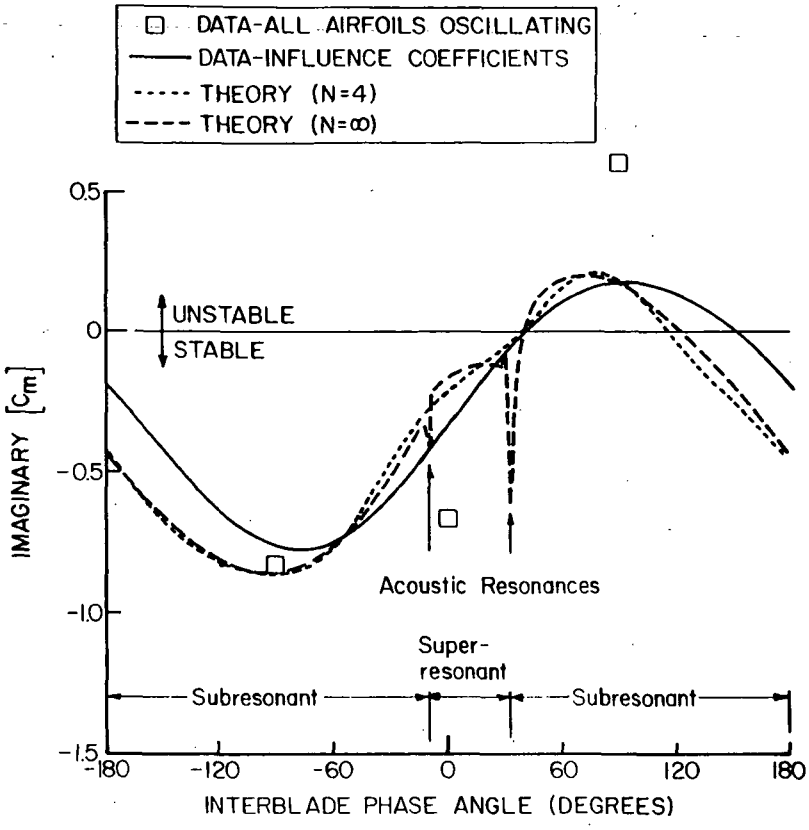

FIGURE 20. - IMAGINARY UNSTEADY AERODYNAMIC MOMENT CORRELATION, k = 0.223.

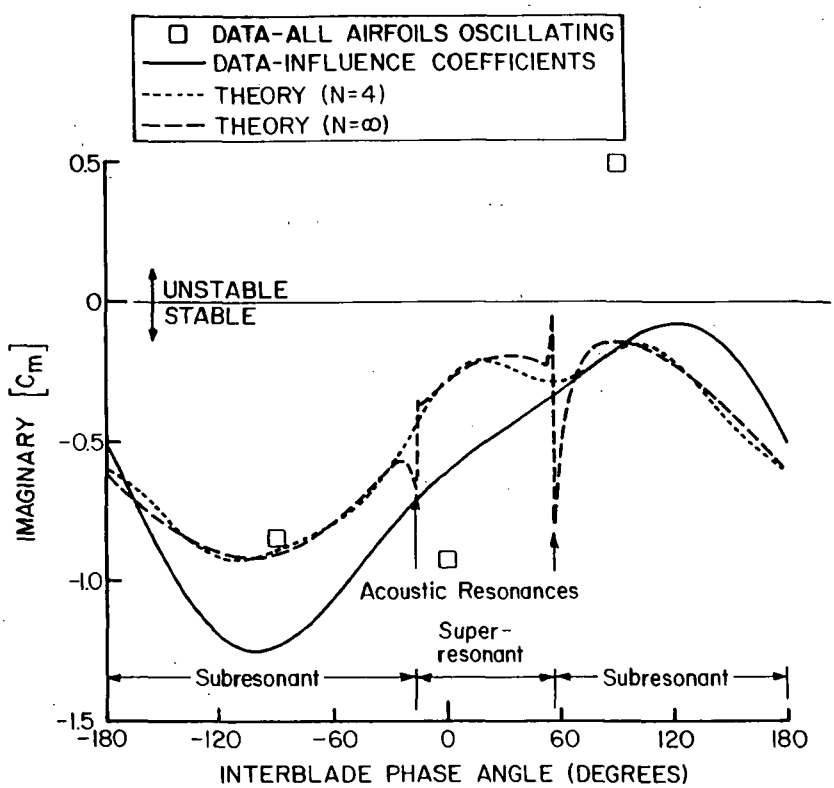

FIGURE 21. - IMAGINARY UNSTEADY AERODYNAMIC MOMENT CORRELATION, k = 0.390.

NASA
National Aeronautics and Space Administration

Report Documentation Page

1. Report No.	2. Government Accession No.	3. Recipient's Catalog No.
NASA TM-101313 AIAA-88-2815		

4. Title and Subtitle

Investigation of Oscillating Cascade Aerodynamics by an Experimental Influence Coefficient Technique

5. Report Date

6. Performing Organization Code

7. Author(s)

Daniel H. Buffum and Sanford Fleeter

8. Performing Organization Report No.

E-4308

10. Work Unit No.

535-03-01

9. Performing Organization Name and Address

National Aeronautics and Space Administration
Lewis Research Center
Cleveland, Ohio 44135-3191

11. Contract or Grant No.

13. Type of Report and Period Covered

Technical Memorandum

12. Sponsoring Agency Name and Address

National Aeronautics and Space Administration
Washington, D.C. 20546-0001

14. Sponsoring Agency Code

15. Supplementary Notes

Presented at the 24th Joint Propulsion Conference cosponsored by the AIAA, ASME, SAE, and ASEE, Boston, Massachusetts, July 11-13, 1988. Daniel H. Buffum, NASA Lewis Research Center; Sanford Fleeter, Thermal Sciences and Propulsion Center, School of Mechanical Engineering, Purdue University, West Lafayette, Indiana 47907.

16. Abstract

Fundamental experiments are performed in the NASA Lewis Transonic Oscillating Cascade Facility to investigate the torsion mode unsteady aerodynamics of a biconvex airfoil cascade at realistic values of the reduced frequency for all interblade phase angles at a specified mean flow condition. In particular, an unsteady aerodynamic influence coefficient technique is developed and utilized in which only one airfoil in the cascade is oscillated at a time and the resulting airfoil surface unsteady pressure distribution measured on one dynamically instrumented airfoil. The unsteady aerodynamics of an equivalent cascade with all airfoils oscillating at a specified interblade phase angle are then determined through a vector summation of these data. These influence coefficient determined oscillating cascade data are correlated with data obtained in this cascade with all airfoils oscillating at several interblade phase angle values. The influence coefficients are then utilized to determine the unsteady aerodynamics of the cascade for all interblade phase angles, with these unique data subsequently correlated with predictions from a linearized unsteady cascade model.

17. Key Words (Suggested by Author(s))	18. Distribution Statement
Unsteady aerodynamics Cascade flow Flutter	Unclassified - Unlimited Subject Category 02

19. Security Classif. (of this report)	20. Security Classif. (of this page)	21. No of pages	22. Price*
Unclassified	Unclassified	24	A03

NASA FORM 1626 OCT 86

*For sale by the National Technical Information Service, Springfield, Virginia 22161